AAS 21-639

AUTONOMOUS CROSS-CALIBRATION FOR IMAGING SATELLITES

Zvonimir Stojanovski* **and Dmitry Savransky†**

We present a fully autonomous image-based cross-calibration method for constellations of Earth-observing satellites. Here, each satellite extracts features from primary mission images and then transmits the features, along with its state estimate, to other satellites. Furthermore, each satellite uses comparisons of the image features, along with conventional state measurements, to estimate its position, attitude, and camera parameters via the unscented Kalman filter or the higher-order unscented estimator. We demonstrate the simulation framework for testing this method with an example featuring two imaging satellites. In the future, we will rigorously test the method's performance and refine the image-based measurement model.

INTRODUCTION

Cross-calibration between satellites is crucial to the performance of Earth-observing constellations. To this end, very rigorous cross-calibration schemes have been developed and implemented, e.g., for the Dove constellation.[1] However, these techniques rely heavily on communications with the ground station and humans-in-the-loop. As a result, they may not be feasible for larger constellations. Furthermore, state-of-the art in-situ sensor calibration techniques, such as those used for the Lunar Reconnaissance Orbiter (LRO)[2] and the GaoFen4 geostationary optical imaging satellite,[3] rely on dedicated calibration measurements and accurate position and attitude estimates. To mitigate some of these difficulties, we propose a method called Autonomous Cross-Calibration for Imaging Satellites (ACCIS). This method uses measurements obtained from the primary mission images, combined with conventional position and attitude measurements, to estimate the states of satellites and their cameras, with key data transmitted between satellites to achieve accurate cross-calibration. In this paper, we will describe in detail the concept of operation for ACCIS and demonstrate its operation in a realistic simulation.

In ACCIS, each satellite computes a real-time estimate of its state, which includes its position, attitude, and camera parameters, which is done using a nonlinear filter. The filter processes not only conventional position and attitude measurements, but also measurements obtained from images. Specifically, it uses features, or key points, extracted from

*PhD Candidate, Sibley School of Mechanical and Aerospace Engineering, Cornell University, 404 Upson Hall, Ithaca, NY 14853.

†Associate Professor, Sibley School of Mechanical and Aerospace Engineering, Cornell University, 451 Upson Hall, Ithaca, NY 14853.

images using the Scale-Invariant Feature Transform (SIFT) introduced by Lowe.[4] For each key point found in the image, the SIFT algorithm computes a position, orientation, and scale, as well as a descriptor that is invariant under translation, rotation, and scaling. This allows us to develop a measurement model that maps changes in the imaging satellite's position, attitude, and camera parameters to changes in a key point's position, orientation, and scale.

For filtering, ACCIS uses either the Unscented Kalman Filter (UKF), developed by Julier and Uhlmann,[5] or the Higher-Order Unscented Estimator (HOUSE), developed by the authors[6] with the application of satellite cross-calibration in mind. The former is known to be robust and computationally efficient for a wide range of systems with nonlinear dynamics and measurements.[7] The latter is an extension of the UKF that accounts for third and fourth order moments—i.e., skewness and kurtosis—in addition to the mean and covariance, allowing more accurate estimation in systems with non-Gaussian noise.[6] This is particularly relevant for measurements based on features extracted from satellite imagery, which exhibit highly non-Gaussian error.[8]

During a mission, ACCIS would operate as follows. Whenever a satellite takes an image, it extracts the key points using SIFT. It then transmits the key points, along with the state estimate and covariance from its observer, to other satellites in the constellation. Then, when two or more satellites have imaged approximately the same area, each of them can use the difference in the key points and the estimated states to update its own state estimate.

Compared to existing techniques, ACCIS has several features that could make cross-calibration faster and cheaper for large constellations of imaging satellites. First, it is fully autonomous, requiring no humans-in-the-loop. Also, it does not require uplinks or downlinks, but only crosslinks between satellites, reducing the communication load for the ground station. Furthermore, the crosslinks transmit only the state estimates, covariance matrices, and SIFT key points and descriptors, which is much less expensive than transmitting full images. In addition, this method uses only the primary mission data, requiring no dedicated calibration measurements.

To test the performance of ACCIS, we develop a detailed simulation framework. In the simulation, each of the satellites is equipped with a GPS receiver, a star tracker, and a nominally nadir-pointing camera for imaging. The simulation features a detailed model of the satellites' rigid-body attitude dynamics and orbital motion, including high-fidelity models for perturbations such as non-spherical Earth gravity and aerodynamic drag. We also model the orientation, focus, and distortion parameters of the satellites' cameras. To emulate the raw data obtained by the satellites, we generate synthetic images from Landsat data; a mosaic formed from Landsat images is trimmed, projected, and distorted based on the satellites' position, field of view, and camera distortion parameters.

The rest of the paper is organized as follows. First, we describe the state model of a satellite, including both its dynamics and camera parameters. Then, we describe the measurement models, including conventional state measurements and novel image-based measurements. After that, we provide a summary of the filtering techniques used. Finally, we present preliminary results showing the operation of the simulation framework.

STATE MODELS

In ACCIS, the satellite state is considered to include both its dynamical state and its camera parameters. In this section, we describe all of the state components, how they are propagated in time, and how they relate to the imaging operations of the satellite.

Satellite Dynamics

We model each satellite as a rigid body in a perturbed Keplerian orbit. Let G denote the satellite's center of mass and O the center of the Earth. Furthermore, let $\mathscr{I}$ denote an Earth-centered inertial (ECI) frame and $\mathscr{B}$ a body-fixed frame. To simplify calculations, we choose $\mathscr{B}$ to be the principal axis frame, though in theory any other body-fixed frame could be used. The satellite's dynamical state consists of the position $\mathbf{r}_{G/O}$, velocity $\mathbf{v}^{\mathscr{I}}_{G/O}$, attitude quaternion $\mathbf{q}_{\mathscr{B}/\mathscr{I}}$, and angular velocity $\boldsymbol{\omega}_{\mathscr{B}/\mathscr{I}}$. The translational dynamics of the satellite are governed by

$$\dot{\mathbf{v}}^{\mathscr{I}}_{G/O} = \mathbf{g} + \mathbf{u}_G + \mathbf{f}_G, \tag{1}$$

where $\mathbf{g}$ is the gravitational acceleration, $\mathbf{u}_G$ is acceleration due to controls (e.g., thrusters), and $\mathbf{f}_G$ is the sum of all other perturbing forces, including atmospheric drag. The rotational dynamics of the satellite are governed by

$$\dot{\boldsymbol{\omega}}^{\mathscr{B}}_{\mathscr{B}/\mathscr{I}} = \mathbb{I}^{-1}(\mathbf{M}_G + \boldsymbol{\tau}_G - \boldsymbol{\omega}_{\mathscr{B}/\mathscr{I}} \times (\mathbb{I}_G \cdot \boldsymbol{\omega}_{\mathscr{B}/\mathscr{I}})) \tag{2}$$

where $\mathbb{I}_G$ is the inertia tensor of the satellite about G, $\mathbf{M}_G$ is the total control moment due to ADCS actuators, and $\boldsymbol{\tau}_G$ is the total disturbance torque. In the filter, we model $\mathbf{f}_G$ and $\boldsymbol{\tau}_G$ as random process noise, due to the difficulty of accurately predicting the atmospheric density, the satellite's aerodynamics properties, and other factors.

For the Earth's gravitational field, we use a truncated version of the EGM2008,[9] with the gravitational forces evaluated using the procedures described Gottlieb.[10] For transformations between the ECI frame and the Earth-centered Earth-fixed frame (ECEF), we use the Naval Observatory Vector Astronomy Subroutines (NOVAS).[11] When propagating the "ground truth" state in the simulation, we compute drag forces using the NRLMSISE-00 atmospheric model.[12]

Camera Model

Let P be an arbitrary point in the camera's field of view. In an ideal pinhole camera at point C, this point is projected onto a point P' in the image plane, at the focal distance u from the camera origin and opposite of C. In a real camera, on the other hand, P is projected onto a different point P'' due to distortions. For simplicity, we assume a purely radial distortion model, i.e., that the positions $\mathbf{r}_{P'}$ and $\mathbf{r}_{P''}$ satisy

$$\frac{\mathbf{r}_{P'}}{\|\mathbf{r}_{P'}\|} = \frac{\mathbf{r}_{P''}}{\|\mathbf{r}_{P''}\|}. \tag{3}$$

Such models are widely used to correct distortions in commercial lenses.[13] Specifically, we use a third-order radial distortion model,

$$\|\mathbf{r}_{P''}\| = \|\mathbf{r}_{P'}\| \left(1 - c_1 - c_2 - c_3 + c_1 \frac{\|\mathbf{r}_{P'}\|}{R} + c_2 \frac{\|\mathbf{r}_{P'}\|^2}{R^2} + c_3 \frac{\|\mathbf{r}_{P'}\|^3}{R^3}\right), \tag{4}$$

where c_1, c_2, and c_3 are the distortion parameters for a particular lens, and R is the radius a circle circumscribed about the image; that is,

$$R = \frac{1}{2}\sqrt{W^2 + L^2}, \tag{5}$$

where W and L are the width and length of the image, respectively. This scaling ensures that the distortion parameters are of the same order of magnitude, which improves numerical stability in the filter. Furthermore, for filtering purposes, we combine the distortion parameters into a vector $\mathbf{c} = \begin{bmatrix} c_1 & c_2 & c_3 \end{bmatrix}^{\mathrm{T}}$.

In addition to the distortion, we account for imperfect focusing of the camera. This depends on the focal length f of the lens, the aperture size A, the distance u from the camera to the object, and the density ρ of pixels per unit length. The effects of defocusing can be modeled well by a Gaussian blur with standard deviation[14]

$$\sigma_G = \frac{\sigma}{\sqrt{2}}, \tag{6}$$

where

$$\sigma = \rho \frac{fs}{2N}\left(\frac{1}{f} - \frac{1}{u} - \frac{1}{s}\right) \tag{7}$$

and

$$N = \frac{f}{A}. \tag{8}$$

Finally, we account for the fact that the orientation of the camera frame $\mathscr{C}$ with respect to the body frame $\mathscr{B}$ is not known exactly, e.g., due to structural tolerances. We parametrize this attitude by a quaternion $\mathbf{q}_{\mathscr{C}/\mathscr{B}}$.

All of the camera parameters that are estimated by the filter—namely, $\mathbf{c}$, f, and $\mathbf{q}_{\mathscr{C}/\mathscr{B}}$—are assumed to be constant in time. Therefore, in the filter they are modeled as having unity dynamics with zero process noise. In the future, we will add a noise term to account for drift in the parameters, particularly for $\mathbf{q}_{\mathscr{C}/\mathscr{B}}$.

In the simulation, we generate synthetic satellite images based on Landsat data and our camera model. Specifically, we obtain a sector of a Landsat image mosaic using the NASA World Wind library.[15] Then, we apply a perspective transform, based on the satellite's position, attitude, and camera parameters. Finally, we apply the radial distortion and defocusing blur. For the transform, distortion, and blurring, we use the OpenCV library.[16]

Combined State

By combining the dynamical state of the satellite with the camera parameters, we obtain the overall system state that is estimated by the filter in ACCIS:

$$\mathbf{x} = \begin{bmatrix} \mathbf{r}_{G/O}{}^{\mathrm{T}} & \mathbf{v}_{G/O}^{\mathscr{I}}{}^{\mathrm{T}} & \boldsymbol{\omega}_{\mathscr{B}/\mathscr{I}}{}^{\mathrm{T}} & \mathbf{q}_{\mathscr{B}/\mathscr{I}}{}^{\mathrm{T}} & \mathbf{q}_{\mathscr{C}/\mathscr{B}}{}^{\mathrm{T}} & f & \mathbf{c}^{\mathrm{T}} \end{bmatrix}^{\mathrm{T}}. \tag{9}$$

The system state has a total of 21 components. While the rates $\mathbf{v}_{G/O}^{\mathscr{I}}$ and $\boldsymbol{\omega}_{\mathscr{B}/\mathscr{I}}$ are not necessary for image calibration (assuming sufficiently short exposure time), they are needed for state prediction in the filter.

MEASUREMENT MODELS

The ACCIS framework features two categories of measurements: conventional measurements of the satellite's dynamical states and measurements derived from images.

Conventional Measurements

In our model, the satellite is equipped with a Global Positioning System (GPS) receiver, which provides measurements of its position and velocity, and also a star tracker to obtain precise attitude measurements. The GPS measurements are assumed to have a Gaussian noise distribution. The star tracker measurements are assumed to have a boresight error and a normal error, also with a Gaussian distribution.

Image-Based Measurements

While straightforward models exist for the conventional measurements, there are no standard methods for relating image data to the satellite's dynamical state and camera parameters. Here, we present a preliminary model for measurements based on features extracted from images.

The Scale-Invariant Feature Transform (SIFT), proposed by Lowe,[4] provides a robust and efficient method for extracting and matching features from images. Each feature, or key point, extracted from an image by SIFT includes a position $\mathbf{r}_K$, orientation angle θ, and scale S, as well as a gradient-based descriptor that is invariant under translation, rotation, and scaling. Also, the effects of differences in illumination and perspective are relatively small. Thus, the descriptors can be matched between images taken from various distances, angles, etc. However, the SIFT descriptors not fully invariant under affine transformations. In the simulation, we use the implementation of SIFT from the OpenCV library.[16]

To make the SIFT key points more convenient to use in our model, we use an equivalent representation as two positions, $\mathbf{r}_{K_1'}$ and $\mathbf{r}_{K_2'}$, given by

$$\mathbf{r}_{K_{1,2}'} = \mathbf{r}_K \pm \frac{1}{2} S\mathbf{u}, \tag{10}$$

where $\mathbf{u} = \begin{bmatrix} \cos\theta & \sin\theta \end{bmatrix}^{\mathrm{T}}$. Thus, a key point is given by

$$\mathbf{K} = \begin{bmatrix} \mathbf{r}_{K_1'}^{\mathrm{T}} & \mathbf{r}_{K_2'}^{\mathrm{T}} \end{bmatrix}^{\mathrm{T}}, \tag{11}$$

and we can directly convert between this and the standard key point representation. Given the time t and the satellite state $\mathbf{x}$, we can geometrically map $\mathbf{r}_{K_i'}$ to a point on the Earth's surface and vice versa. For this, we take into account the position and attitude of the satellite, as well as the attitude, distortion, etc. of the camera.

Suppose that a descriptor matching algorithm has matched two key points $\mathbf{K}_1$ and $\mathbf{K}_2$, from images taken at times t_1 and t_2 by satellites with states $\mathbf{x}_1$ and $\mathbf{x}_2$, respectively. We can map $\mathbf{K}_1$ to a pair of points on Earth's surface given t_1 and $\mathbf{x}_1$. Then, given t_2 and $\mathbf{x}_2$, we can map two ground positions to a "predicted" key point $\hat{\mathbf{K}}_2$. Thus, given estimate distributions of $\mathbf{x}_1$ and $\mathbf{x}_2$, we can obtain a distribution of $\hat{\mathbf{K}}$, adding an error term to both $\mathbf{K}_1$ and $\hat{\mathbf{K}}_2$. Then, we can apply $\mathbf{K}_2$ as the "true" measurement in the filter update step, to obtain a better estimate of $\mathbf{x}_2$.

In the future, we will expand this method to more accurately model the relation between the satellite state and the SIFT key points. In particular, we will investigate how the gradient-based descriptors could be used as part of the state measurement and not only for key point matching.

FILTERING METHODS

The discrete-time nonlinear filtering problem can be summarized as follows, and the description of the satellite state and measurements in the previous two sections can easily be cast in the above form. A system with state $\mathbf{x}$ evolves in time as

$$\mathbf{x}(k+1) = \mathbf{f}(\mathbf{x}(k), \mathbf{u}(k), \mathbf{w}(k), k), \tag{12}$$

where k is the time step, $\mathbf{u}$ is the control, $\mathbf{w}$ is the process noise, and $\mathbf{f}$ is a nonlinear function. We want to find an estimate of $\mathbf{x}(K)$ based on a sequence of measurements $\mathbf{z}(0), \mathbf{z}(1), \ldots, \mathbf{z}(K)$, given by

$$\mathbf{z}(k) = \mathbf{h}(\mathbf{x}(k), \mathbf{n}(k), k), \tag{13}$$

where $\mathbf{n}$ is the measurement noise, and $\mathbf{h}$ is a nonlinear function. Note that $\mathbf{h}$ may have very different characteristics for different values of k, e.g., if different types of measurements are taken at different cadences.

The Unscented Kalman Filter

The unscented Kalman filter (UKF), proposed by Julier and Uhlmann,[5] is based on the unscented transform (UT), in which the distribution of the state $\mathbf{x} \in \mathbb{R}^n$ is approximated by a set of $2n+1$ points $\mathbf{x}_j$, called sigma points, with weights w_j. The points are given by

$$\mathbf{x}_j = \begin{cases} \bar{\mathbf{x}} + \sqrt{n+\kappa}\mathbf{c}_j, & 1 \le j \le n \\ \bar{\mathbf{x}} - \sqrt{n+\kappa}\mathbf{c}_{j-n}, & n+1 \le j \le 2n \\ \bar{\mathbf{x}}, & j = 2n+1 \end{cases} \tag{14}$$

where $\mathbf{c}_j$ is the j-th column of $\sqrt{\mathbf{P}_{xx}}$, and κ is a tuning factor. The matrix square root is not unique; it is most often evaluated using the Cholesky decomposition, though other

methods, such as eigenvalue decomposition, may also be used. The corresponding weights are given by

$$w_j = \begin{cases} \frac{1}{2(n+\kappa)}, & 1 \leq j \leq 2n \\ \frac{\kappa}{n+\kappa} & j = 2n+1 \end{cases} \tag{15}$$

Then, for an arbitrary nonlinear function $\phi : \mathbb{R}^n \to \mathbb{R}$, we can approximate the expected value $\mathrm{E}[\phi(\mathbf{x})]$ by a weighted sum over the sigma points:

$$\mathrm{E}[\phi(\mathbf{x})] \approx \sum_{j=1}^{2n+1} w_j \phi(\mathbf{x}_j). \tag{16}$$

Such approximations are used for the mean and covariance of the predicted state in the filter's prediction step and the measurement in the filter's update step.

The Higher-Order Unscented Estimator

The authors developed an extension of the UKF, called the Higher-Order Unscented Estimator (HOUSE), which accounts for third and fourth order moments in addition to the mean and covariance.[6] Specifically, HOUSE uses a modified unscented transform that preserves the skewness and kurtosis (the marginal third and fourth order moments) of the standardized state $\tilde{\mathbf{x}}$, which is defined as

$$\tilde{\mathbf{x}} = \left(\sqrt{\mathbf{P}_{xx}}\right)^{-1} (\mathbf{x} - \bar{\mathbf{x}}), \tag{17}$$

which has a mean of zero and a covariance equal to the identity matrix. Let γ_j and κ_j denote the skewness and kurtosis of $\tilde{x}_j$, respectively. The sigma points in HOUSE are given by

$$\mathbf{x}^{(j)} = \begin{cases} \bar{\mathbf{x}} + \alpha_j \mathbf{c}^{(j)}, & 1 \leq j \leq n \\ \bar{\mathbf{x}} - \beta_{j-n} \mathbf{c}^{(j-n)} & n+1 \leq j \leq 2n \\ \bar{\mathbf{x}} & j = 2n+1 \end{cases} \tag{18}$$

where

$$\alpha_j = \frac{\gamma_j + \sqrt{4\kappa_j - 3\gamma_j^2}}{2} \tag{19}$$

and

$$\beta_j = \frac{-\gamma_j + \sqrt{4\kappa_j - 3\gamma_j^2}}{2}. \tag{20}$$

Due to Pearson's inequality,

$$\kappa_j \geq \gamma_j^2 + 1, \tag{21}$$

the coefficients α_j and β_j are guaranteed to be real and positive. The corresponding weights are given by

$$w_j = \begin{cases} \frac{1}{\alpha_j^2 + \alpha_j \beta_j}, & 1 \leq j \leq n \\ \frac{1}{\beta_{j-n}^2 + \alpha_{j-n} \beta j-n}, & n+1 \leq j \leq 2n \\ 1 - \sum_{i=1}^{n} \frac{1}{\alpha_i \beta_i} & j = 2n+1 \end{cases} \tag{22}$$

All weights except w_{2n+1} are guaranteed to be positive. However, even one negative weight can be problematic; for example, it can generate a covariance matrix that is not positive-definite. To ensure that $w_{2n+1} > \delta$ for some $\delta \geq 0$, we can modify the kurtosis to take the value

$$\kappa_i' = \begin{cases} \kappa_{\min}, & \kappa \leq \kappa_{\min} \\ \kappa_i, & \kappa > \kappa_{\min} \end{cases} \tag{23}$$

where

$$\kappa_{\min} = \frac{n}{1-\delta}. \tag{24}$$

The computational complexity of HOUSE is not significantly greater than that of the conventional UKF, since both filters require $2n+1$ sigma points; the runtimes for HOUSE were found to be only slightly longer than for the UKF.[6] Another higher-order estimator is the Conjugate Unscented Transform (CUT) filter proposed by Adurthi, Singla, and Singh, which uses $O(2^n)$ sigma points to match moments for a specific family of distributions (e.g., Gaussian or uniform) up to the fourth, sixth, or eighth order.[17] While CUT filters can provide more accurate estimates than the conventional UKF or HOUSE in cases with Gaussian noise,[6] the dimension of the satellite state makes CUT infeasible for the satellite cross-calibration problem, as it would require more than $2^{21} = 2,097,152$ sigma points.

As for estimation accuracy, the main advantage of HOUSE is robustness in the presence of outliers in the process and measurement noise. Numerical tests show that HOUSE produces much fewer outliers in the estimation error, compared to the UKF and CUT filter, when the process and measurement noise have a high kurtosis and are therefore more likely to produce outliers. In such cases, the root-mean-square error (RMSE) is found to be significantly lower for the other filters. In cases with Gaussian noise, the accuracy of HOUSE was found to be comparable to that of the UKF.[6]

PRELIMINARY RESULTS

As an initial test of the ACCIS framework, we ran a short simulation of two Earth-observing satellites. The two satellites are in circular, equatorial orbits at an altitude of 400 km, with a 0.5° difference in true anomaly. Each is equipped with a nominally nadir-pointing camera, with a nominal focal length of 2000 mm, an aperture of 500 mm, and an image size of 1000×1000 pixels, with a density of 1 pixel/mm.

At $t = 5$ s, each satellite takes an image, extracts the key points using SIFT, and transmits its state estimate and the key points to the other satellite. Then, at $t = 15$ s, each satellite takes another image, applies SIFT to it, and updates its state estimate using the new key points and the prior data from the other satellite. Throughout the simulation, each satellite obtains GPS and star tracker measurements at a cadence of 5 Hz.

Figure 1 shows the images obtained by the two satellites, showing the overlap between the image frames. Figures 2 and 3 show the error in the dynamical state estimate for the UKF and HOUSE, respectively, and Figures 4 and 5 show the error in the camera parameter estimates. The dynamical state error is nearly equal for the two filters, most likely because

Time (s)	Satellite 1	Satellite 2
5	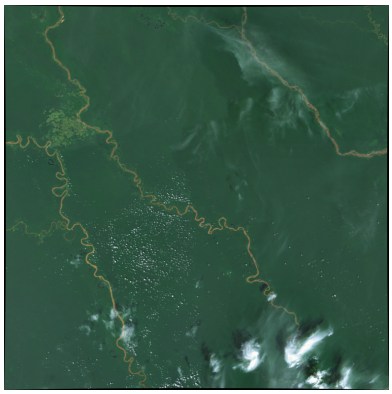	
15	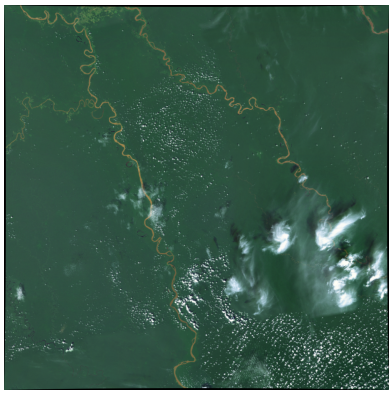	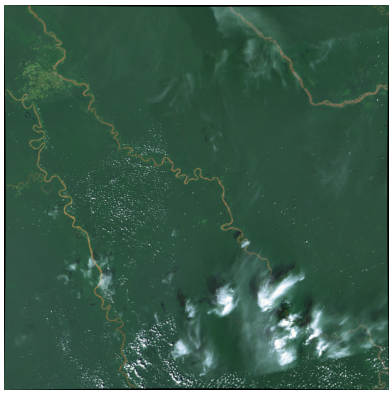

Figure 1. Images captured by the two satellites in the simulation.

the measurement noise is Gaussian. For the camera parameters, on the other hand, the HOUSE error is slightly lower overall. In this test, the image-based measurements do not significantly improve the camera parameter estimates for either filter; they even increase the error for some of the parameters. However, since this test includes only one set of image-based measurements, we cannot draw conclusions on the performance of the filters or the measurement model. A rigorous test of the estimation accuracy of ACCIS will require running the simulation for multiple orbital periods with various orbit and camera parameters. This will be the next step in our work.

CONCLUSION

We have presented a method for the autonomous cross-calibration of imaging satellites, using nonlinear filtering combined with image feature extraction. Also, we have demonstrated that the simulation framework for testing this method is fully operational. In our future work, we will test the performance of ACCIS with longer and more varied simulations, and we will use the results of these simulations to further refine the image-based measurement model. While ACCIS is still a work in progress, we believe that it has the potential to make cross-calibration more accurate and efficient in future missions.

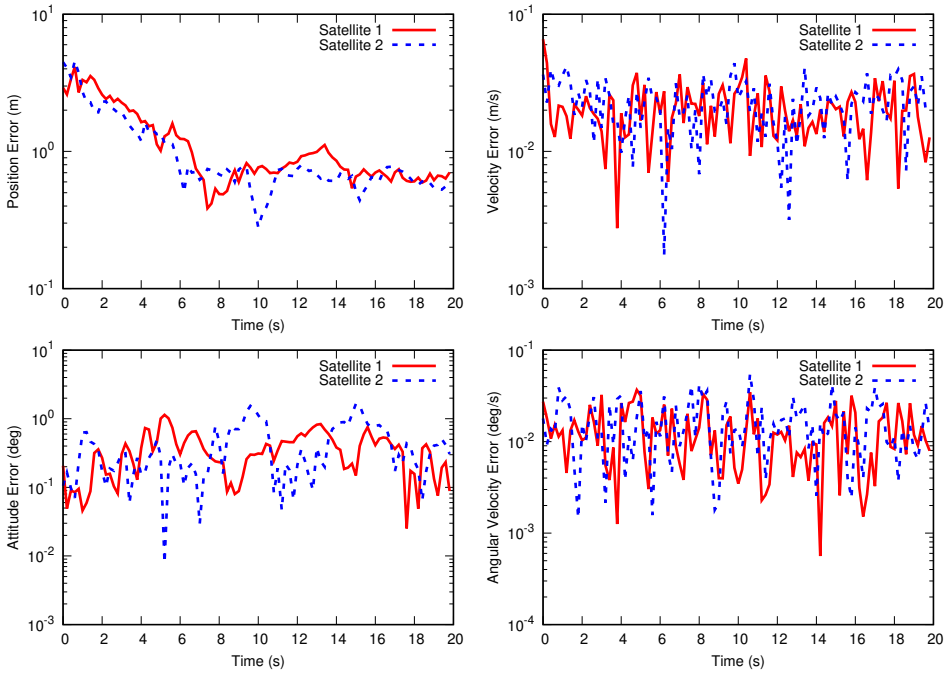

Figure 2. Estimation error for dynamical state using UKF.

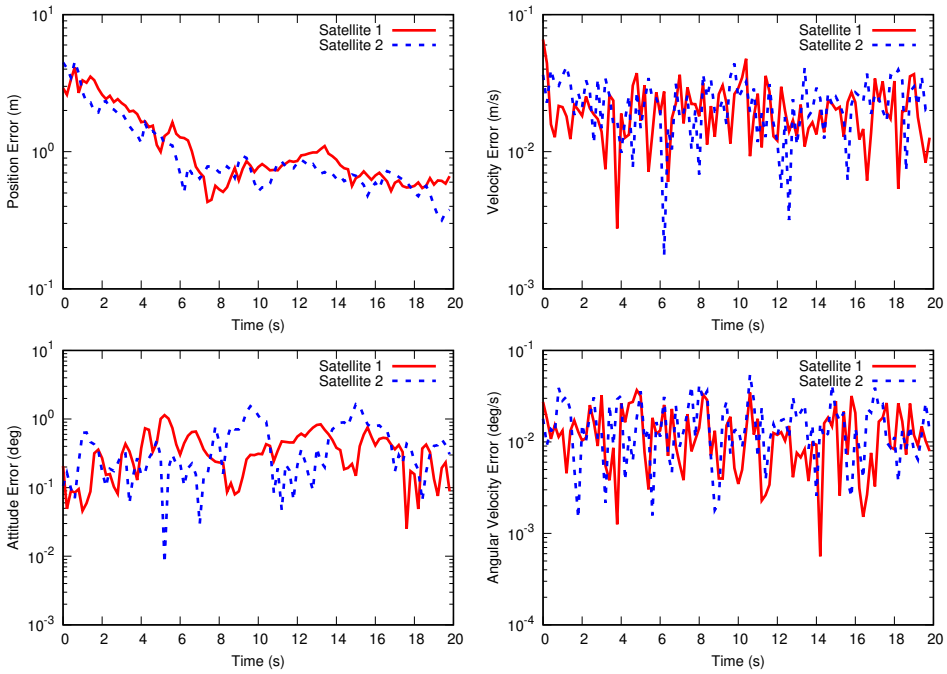

Figure 3. Estimation error for dynamical state using HOUSE.

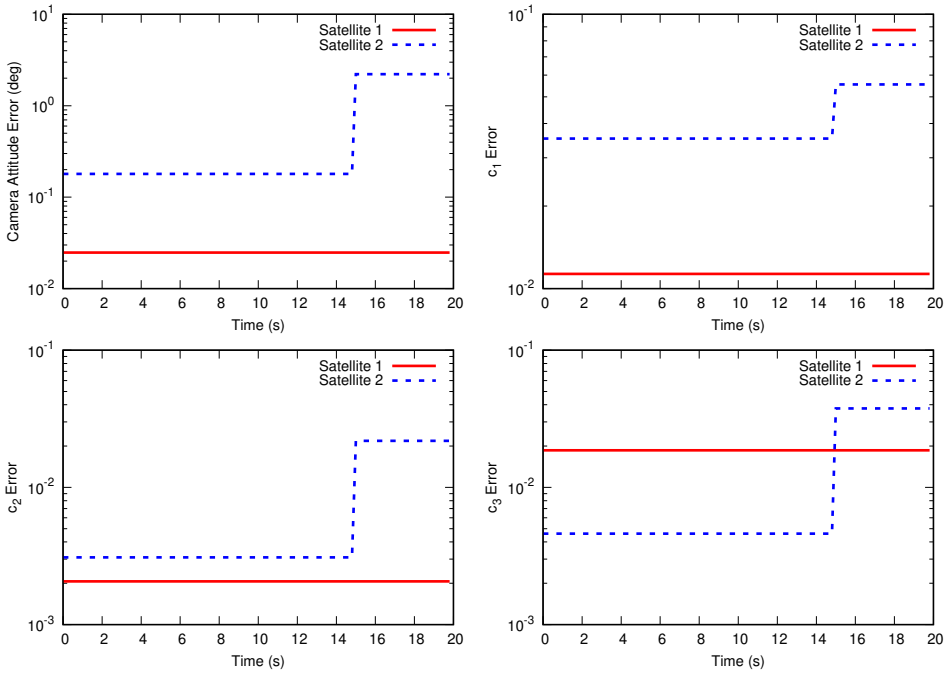

Figure 4. Estimation error for camera parameters using UKF.

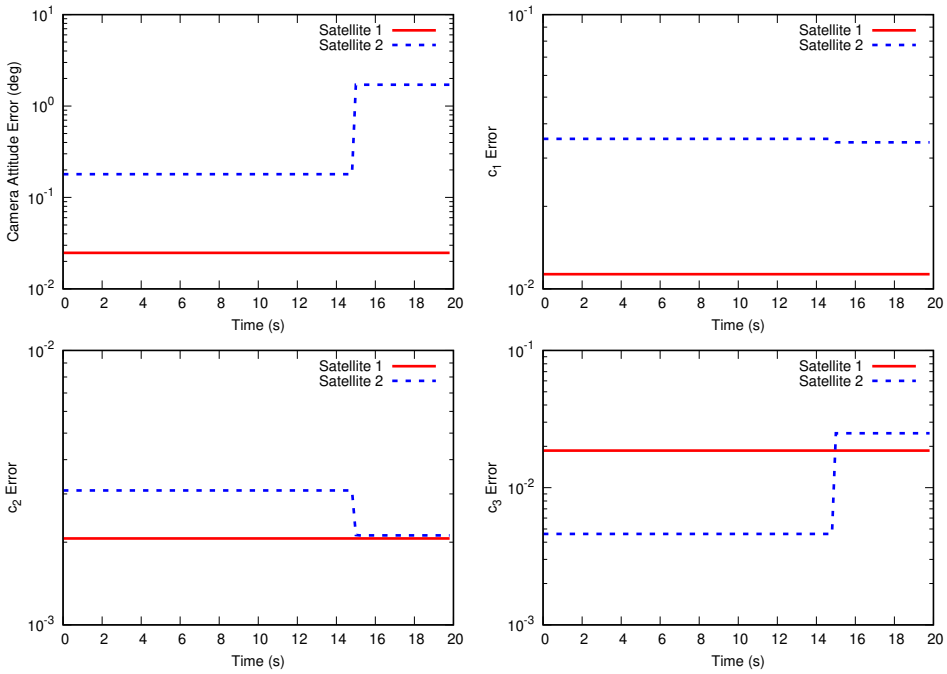

Figure 5. Estimation error for camera parameters using HOUSE.

ACKNOWLEDGEMENTS

The authors acknowledge support for this work from the NASA Space Technology Research Grants Early Career Faculty program under NASA grant 80NSSC20K0068.

REFERENCES

[1] L. Leung, V. Beukelaers, S. Chesi, *et al.*, "ADCS at Scale: Calibrating and Monitoring the Dove Constellation," *32nd Annual AIAA/USU Conference on Small Satellites*, 2018.

[2] E. J. Speyerer, R. V. Wagner, M. S. Robinson, A. Licht, P. C. Thomas, K. Becker, J. Anderson, S. M. Brylow, D. C. Humm, and M. Tschimmel, "Pre-flight and On-orbit Geometric Calibration of the Lunar Reconnaissance Orbiter Camera," *Space Science Reviews*, Vol. 200, 2016, p. 357, https://doi.org/10.1007/s11214-014-0073-3.

[3] M. Wang, Y. Cheng, X. Chang, S. Jin, and Y. Zhu, "On-orbit geometric calibration and geometric quality assessment for the high-resolution geostationary optical satellite GaoFen4," *ISPRS Journal of Photogrammetry and Remote Sensing*, Vol. 125, 2017, pp. 63–77, https://doi.org/10.1016/j.isprsjprs.2017.01.004.

[4] D. G. Lowe, "Distinctive Image Features from Scale-Invariant Keypoints," *International Journal of Computer Vision*, Vol. 60, No. 2, 2004, pp. 91–110.

[5] S. Julier and J. Uhlmann, "A New Extension of the Kalman Filter to Nonlinear Systems," *Proc. SPIE 3068, Signal Processing, Sensor Fusion, and Target Recognition VI*, 1997.

[6] Z. Stojanovski and D. Savransky, "The Higher-Order Unscented Estimator," Accepted to the *Journal of Guidance, Control, and Dynamics*, 2021.

[7] R. Kandepu, B. Foss, and L. Imsland, "Applying the unscented Kalman filter for nonlinear state estimation," *Journal of Process Control*, Vol. 18, No. 7, 2008, pp. 753–768, https://doi.org/10.1016/j.jprocont.2007.11.004.

[8] J. Shapiro, *Using Modern Mathematical and Computational Tools for Image Processing*. PhD thesis, Cornell University, Dec 2020.

[9] N. K. Pavlis, S. A. Holmes, S. C. Kenyon, and J. K. Factor, "An Earth Gravitational Model to Degree 2160: EGM2008," *Presented at the 2008 General Assembly of the European Geosciences Union*.

[10] R. G. Gottlieb, "Fast Gravity, Gravity Partials, Normalized Gravity, Gravity Gradient Torque and Magnetic Field: Derivation, Code and Data,"

[11] G. Kaplan, J. Bartlett, A. Monet, J. Bangert, and W. Puatua, *User's Guide to NOVAS Version F3.1*. United States Naval Observatory, 2011.

[12] J. M. Picone, A. E. Hedin, D. P. Drob, and A. C. Aikin, "NRLMSISE-00 empirical model of the atmosphere: Statistical comparisons and scientific issues," *Journal of Geophysical Research (Space Physics)*, Vol. 107, No. A12, 2002, https://doi.org/10.1029/2002JA009430.

[13] R. G. v. Gioi, Z. Tang, P. Monasse, and J.-M. Morel, "A Precision Analysis of Camera Distortion Models," *IEEE Transactions on Image Processing*, Vol. 26, No. 6, 2017, p. 2694, https://doi.org/10.1109/TIP.2017.2686001.

[14] F. Mannan and M. S. Langer, "What is a Good Model for Depth from Defocus?," *13th Conference on Computer and Robot Vision (CRV)*, 2016, pp. 273–280, https://doi.org/10.1109/CRV.2016.61.

[15] F. Pirotti, M. A. Brovelli, G. Prestifilippo, G. Zamboni, C. E. Kilsedar, M. Piragnolo, and P. Hogan, "An open source virtual globe rendering engine for 3D applications: NASA WorldWind," *Open Geospatial Data, Software and Standards*, Vol. 2, No. 4, 2017, https://doi.org/10.1186/s40965-017-0016-5.

[16] G. Bradski, "The OpenCV Library," *Dr. Dobb's Journal of Software Tools*, 2000.

[17] N. Adurthi, P. Singla, and T. Singh, "Conjugate Unscented Transformation: Applications to Estimation and Control," *Journal of Dynamic Systems, Measurement, and Control*, Vol. 140, No. 3, 2018, pp. 1–22, https://doi.org/10.1115/1.4037783.